

Supramolecular Organization and Charge Transport Properties of Self-Assembled π - π Stacks of Perylene Diimide Dyes

Supplementary Material

Julien Idé, Raphaël Méreau, Laurent Ducasse, Frédéric Castet

*Université de Bordeaux, Institut des Sciences Moléculaires, UMR 5255 CNRS,
351 Cours de la Libération, 33405 Talence, France.*

Yoann Olivier, Nicolas Martinelli, Jérôme Cornil, David Beljonne

*Laboratory for Chemistry of Novel Materials, University of Mons,
Place du Parc 20, B-7000 Mons, Belgium*

1. Supramolecular organization of PDI stacks

1.1. Preparation of the PDI samples

We first performed a minimization at 0K of a large aggregate containing 60 monomers, using $\delta = 0^\circ$, $\theta = 55^\circ$, $d = d_z = 3.5 \text{ \AA}$ and $\Delta X = \Delta Y = 0$ as initial conditions (which correspond to a regular helical stacking where the centers of mass of all monomers are aligned along Z). The evolution of the structural parameters with respect to the position of the monomers along the stack is given in Figure S1. These strongly fluctuate at the outer parts of the columns due to edge effects, while they remain pretty constant in the inner part (between molecule ~20 and ~40). The average values of the structural parameters in this central zone are $\langle d_z \rangle = (3.44 \pm 0.05) \text{ \AA}$, $\langle \theta \rangle = (55.3 \pm 2.0)^\circ$, $\langle |\delta| \rangle = (5.8 \pm 1.0)^\circ$, and the maximal absolute values of the lateral slides ΔX and ΔY are about 2 \AA . The computed $\langle d_z \rangle$ value is consistent with the stacking distances between neighboring molecules reported for several structures of *N,N'*-diphenyl PDI dyes [Klebe_1988].

These first results indicate that the columnar structure exhibits a helical packing of the PDI cores with an average rotation angle θ between the main axes of two adjacent molecules of about 55° . Consequently, a unit cell containing 13 PDI monomers represents 2 complete turns of the helix. Since X-ray diffraction data have shown that the PDI derivative exhibits a hexagonal columnar liquid crystalline phase [Chen_2007], we have next performed MM2 force field calculations using periodic boundary conditions where both atomic positions and lattice parameters have been subjected to minimization. A hexagonal unit cell including 13 PDI units with lattice parameters $a = b = 44 \text{ \AA}$, $c = 45 \text{ \AA}$, $\alpha = \beta = 90^\circ$ and $\gamma = 60^\circ$ was considered as the initial guess to match the length of the alkyl side chain. The minimization leads to final cell parameters $a = 31.54 \text{ \AA}$, $b = 31.31 \text{ \AA}$, $c = 41.82 \text{ \AA}$, $\alpha = 90.1^\circ$, $\beta = 89.7^\circ$ and $\gamma = 63.2^\circ$, which corresponds to a density $\rho = 0.908 \text{ g.cm}^{-3}$.

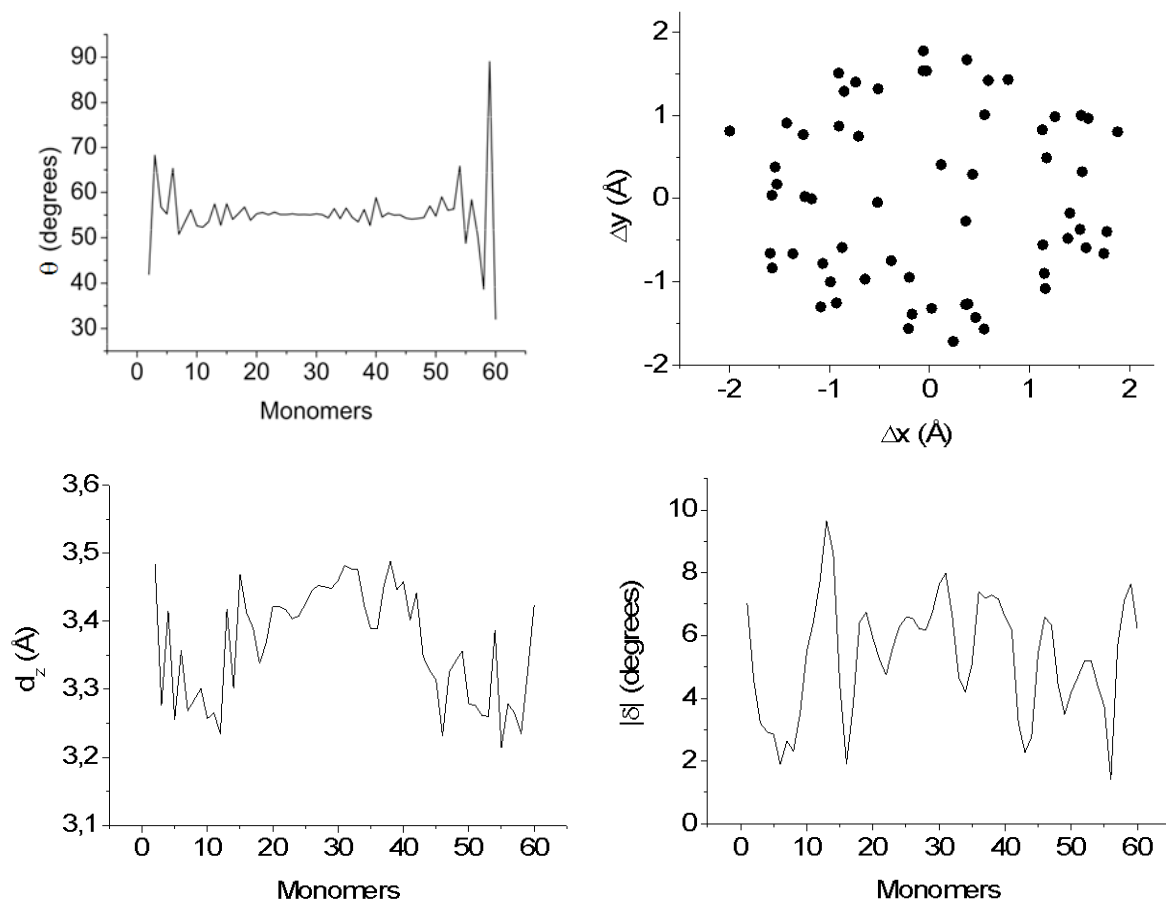


Figure S1: Evolution of the structural parameters with respect to the position of the monomers in the stack, as obtained from a minimization at the MM2 level of an aggregate containing 60 monomers, using $\delta = 0^\circ$, $\theta = 55^\circ$, $d = d_z = 3.5 \text{ \AA}$ and $\Delta X = \Delta Y = 0$ as initial conditions.

1.2. Time evolution of the unit cell density

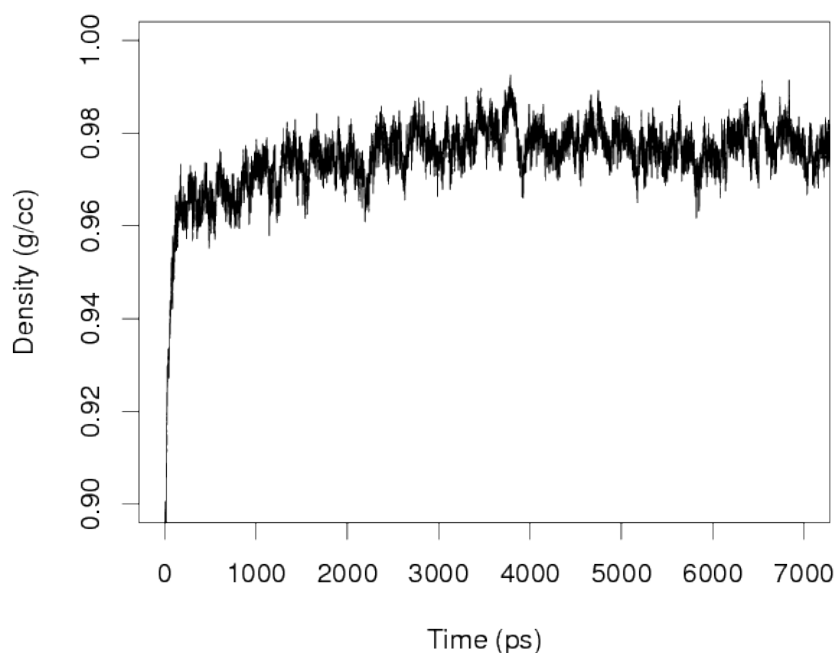


Figure S2: Time evolution of the density of a hexagonal unit cell containing 13 PBI monomers.

2. Calculation of the charge transport parameters

2.1. Simplification of the molecular PBI units

The VB/HF calculations, which are carried out on MD coordinates snapshots to evaluate the impact of the dynamical disorder on the intramolecular and intermolecular charge transport parameters, require to simplify the structure of the PBI stacks. We thus performed preliminary calculations in order to define the molecular fragments giving rise to the best compromise between precision and computational costs. The impact of reducing the complexity of the lateral substituents R has been first investigated, as shown on Figure S3. As charge transport parameters may be significantly affected by polarization effects, the ionization energies, electron affinities and transfer integrals have also been calculated by varying the number of molecular units in the stack (N_{frag}).

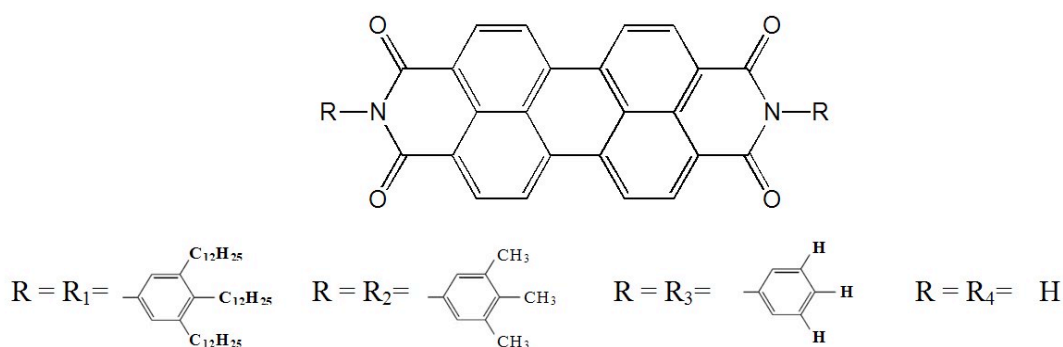


Figure S3: Molecular fragments used in VB/HF calculations

For three structures extracted at arbitrary time steps of the dynamics (200, 600 and 1000 ps), Table S1 reports the IP and EA of the central molecule as a function of N_{frag} and of the nature of the substituent R. The transfer integrals between the two central molecules in the stack are gathered in Table S2 (see Scheme 1 for the labels of the PBI units and the definition of the stacks).

IP												
Time	200				600				1000			
Nfrag	R ₁	R ₂	R ₃	R ₄	R ₁	R ₂	R ₃	R ₄	R ₁	R ₂	R ₃	R ₄
2	8.134	8.145	8.133	8.190	8.189	8.205	8.180	8.254	7.986	7.996	7.994	8.061
5	8.049	8.071	8.060	8.176	7.997	8.035	8.020	8.178	7.883	7.925	7.920	8.039
7	8.037	8.063	8.053	8.193	7.967	8.022	8.010	8.182	7.863	7.903	7.904	8.038
9	8.016	8.041	8.032	8.173	7.965	8.020	8.006	8.193		7.903	7.901	8.049
11		8.047	8.040	8.182		8.022	8.009	8.197		7.900	7.899	8.053
13		8.040	8.035	8.180		8.024	8.012	8.205			7.901	8.054

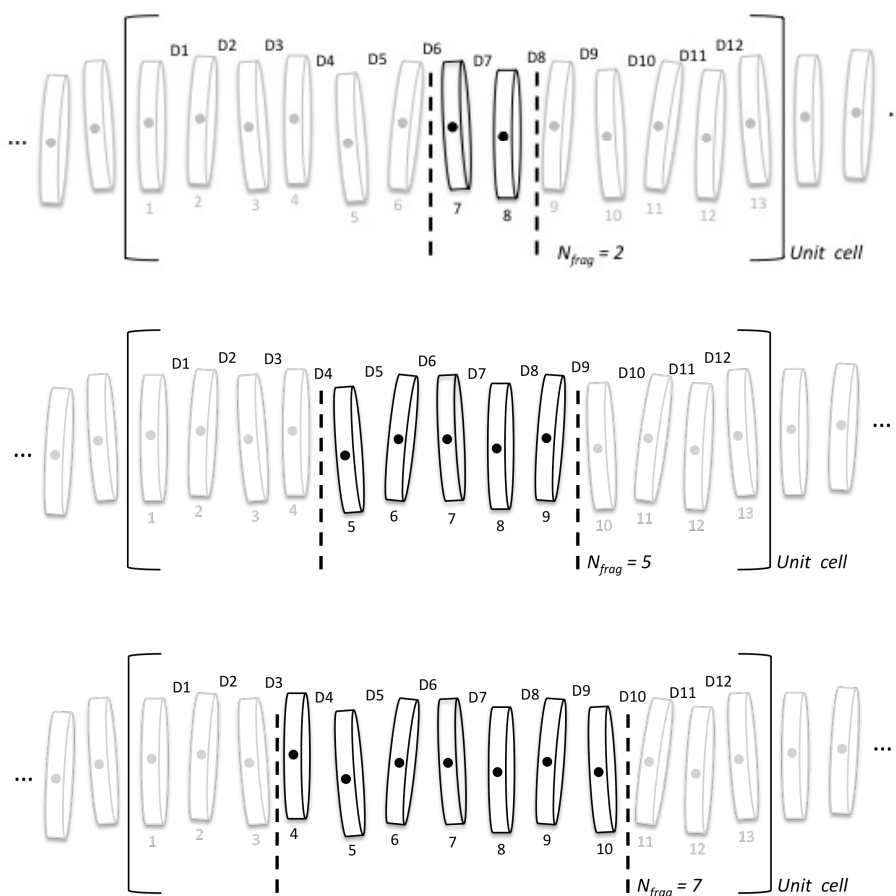
EA												
Time	200				600				1000			
Nfrag	R ₁	R ₂	R ₃	R ₄	R ₁	R ₂	R ₃	R ₄	R ₁	R ₂	R ₃	R ₄
2	3.139	3.077	3.053	2.959	3.305	3.231	3.205	3.109	3.297	3.234	3.217	3.124
5	3.346	3.241	3.208	3.108	3.408	3.307	3.275	3.197	3.489	3.399	3.371	3.272
7	3.399	3.264	3.230	3.137	3.452	3.326	3.294	3.213	3.534	3.409	3.384	3.283
9	3.420	3.258	3.222	3.121	3.494	3.340	3.303	3.229	3.579	3.425	3.396	3.300
11	3.448	3.272	3.238	3.133	3.522	3.351	3.314	3.235		3.431	3.401	3.306
13	3.456	3.271	3.237	3.132	3.533	3.358	3.321	3.244		3.437	3.406	3.308

Table S1: Ionization potential (IP) and electron affinities (EA) (in eV) of the central molecule as a function of the number of units in the stack (N_{frag}) and of the nature of the substituent R, as calculated at the VB/HF-AM1 level for structures extracted at different times of the dynamics.

T-												
Time	200				600				1000			
Nfrag	R ₁	R ₂	R ₃	R ₄	R ₁	R ₂	R ₃	R ₄	R ₁	R ₂	R ₃	R ₄
2	15.930	15.844	15.393	15.295	5.238	4.836	3.772	5.768	48.882	50.131	51.569	49.291
5	15.379	11.912	13.973	12.453	6.330	5.050	2.693	3.826	50.714	51.156	48.644	50.804
7	15.514	14.650	13.379	12.380	6.271	3.845	6.794	3.845	50.262	47.596	48.542	50.805
9	15.089	12.291	12.691	12.416	6.073	4.026	5.566	3.817	50.595	47.876	49.101	47.035
11	13.718	13.822	13.537	12.409	6.383	4.042	6.875	3.822		47.795	48.808	47.040
13	14.465	12.855	12.548	12.414	5.835	3.995	6.883	3.823		50.920	48.840	47.044

T+												
Time	200				600				1000			
Nfrag	R ₁	R ₂	R ₃	R ₄	R ₁	R ₂	R ₃	R ₄	R ₁	R ₂	R ₃	R ₄
2	48.951	55.305	57.350	50.233	82.575	84.120	82.974	85.440	46.888	46.777	43.899	44.088
5	54.634	51.709	44.691	51.890	81.221	84.184	82.595	87.859	41.442	47.818	46.069	41.658
7	46.848	50.635	46.534	51.037	82.772	83.168	83.075	88.350	42.407	47.666	48.435	41.667
9	47.558	49.597	47.550	51.759	82.186	83.011	84.502	88.550		46.325	47.562	41.702
11		51.673	45.813	51.768		83.299	84.453	88.347			47.284	41.707
13		49.518	45.763	51.772		82.630	84.746	88.007				41.712

Table S2: Transfer integrals for electrons (J) and holes (J^{\dagger}) (in meV) between the two central molecules as a function of the number of units in the stack (N_{frag}) and of the nature of the substituent R, as calculated at the VB/HF-AM1 level for structures extracted at different times of the dynamics.



Scheme 1: labels of the PBI units within the unit cell and the definition of the stacks used in the VB/HF calculations.

The same conclusions can be drawn for the three structures. Whatever the nature of the substituent R, the IP (EA) decreases (increases) when increasing the number of units in the stack. Both IP and EA saturate towards asymptotic values, which are reasonably approximated by calculations performed on clusters containing 5 fragments. Replacing the lateral substituent R by a hydrogen atom introduces significant differences in both properties compared to the reference system ($R = R_1$), while calculations performed using a simple phenyl group in R lead to good approximations.

Contrary to IP and EA, the transfer integrals are not significantly impacted by the number of units in the stack, though calculations carried out on the smallest cluster lead to slightly larger deviations. Changing the substituent can have a more significant impact, in particular if one compares the values of J^+ obtained for the system without substituent to the values obtained for the reference system. However, the differences do not exceed 5-6 meV, as expected owing to the fact that transfer integrals mainly originates from the overlap between the molecular orbitals of the perylene cores.

Finally, the transfer integral distributions along the MD run for electrons and holes when the charge migrates from molecule 7 to molecule 8 with $R = R_3 = H$ with and without accounting for environment effects (*i.e.* when considering a dimer isolated ($N_{frag} = 2$) or the same dimer embedded in a larger aggregate ($N_{frag} = 5$), see Scheme 1) are reported in Figures S4 and S5, respectively. The similarity of the two distributions further evidences that polarization effects due to the molecular environment has a negligible impact on the transfer terms.

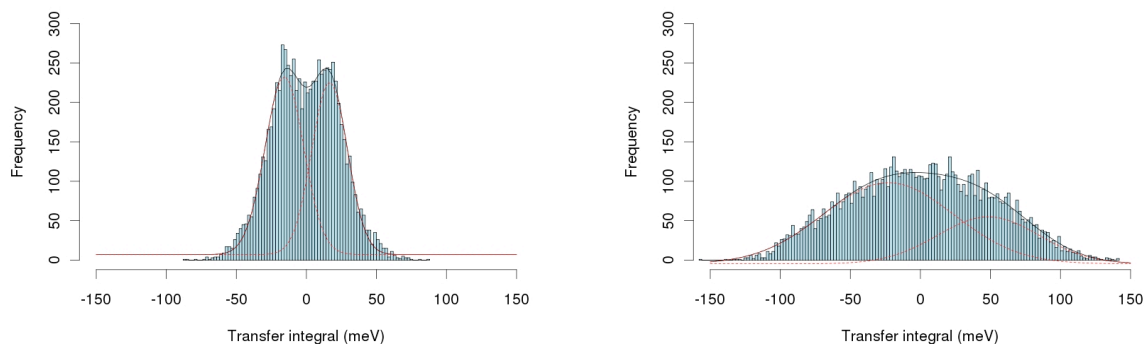


Figure S4: Transfer integral distributions for electrons (left) and holes (right), moving the charge from molecule 7 to molecule 8 within a stack of 5 molecules ($R = H$).

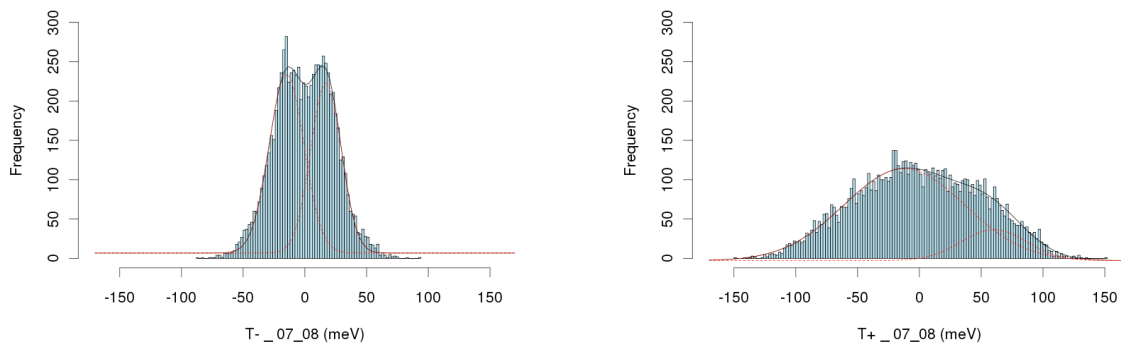


Figure S5: Transfer integral distributions for electrons (left) and holes (right), moving the charge from molecule 7 to the molecule 8 without environment ($R = H$).

2.2. Calculation of the site energies

The distributions of IP and EA of each molecule in the unit cell are reported in Figure S6, where dark areas are associated to large occurrences. All IP/EA distributions display a Gaussian shape. The overall mean values (calculated as the average over the 13 molecules of the average values over the structural samplings) are 7.96 eV for IP and 3.28 eV for EA, while standard deviations are of similar amplitude: $\sigma_{IP} \sim \sigma_{EA} \sim 0.09$ eV. The distributions of the polarization energies P^+ and P^- are portrayed Figure S7, while the changes in P^+ and P^- , associated to the energy disorder along the stack, are illustrated in Figure S8. The distributions of the static $S^{+/-}$ and dynamic $D^{+/-}$ contributions to the polarization energy are portrayed in Figure S9.

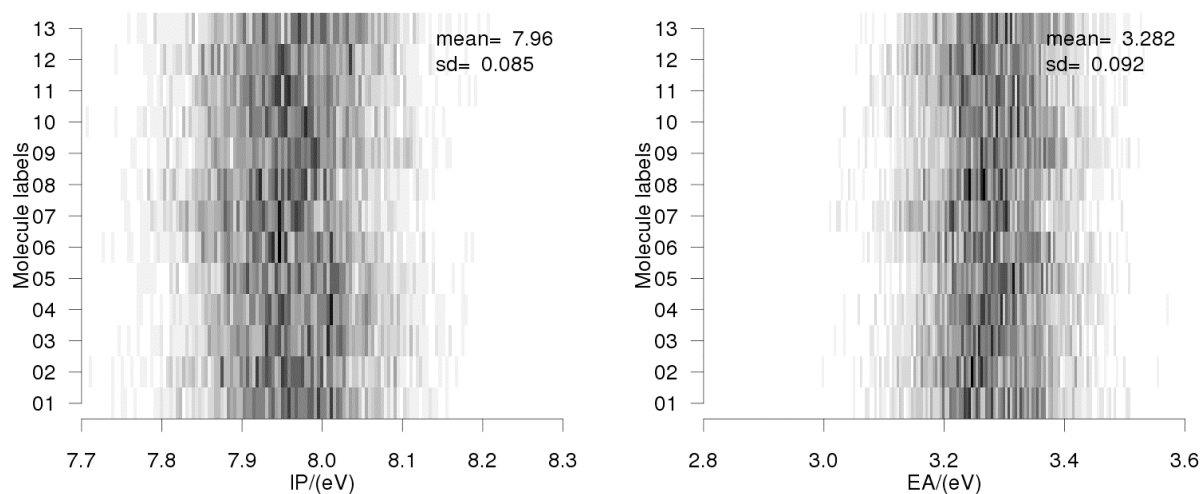


Figure S6: Distributions of IP (left) and EA (right) for each molecule of the unit cell, as calculated at the VB/HF-AM1 level using molecular structures extracted from MD simulations.

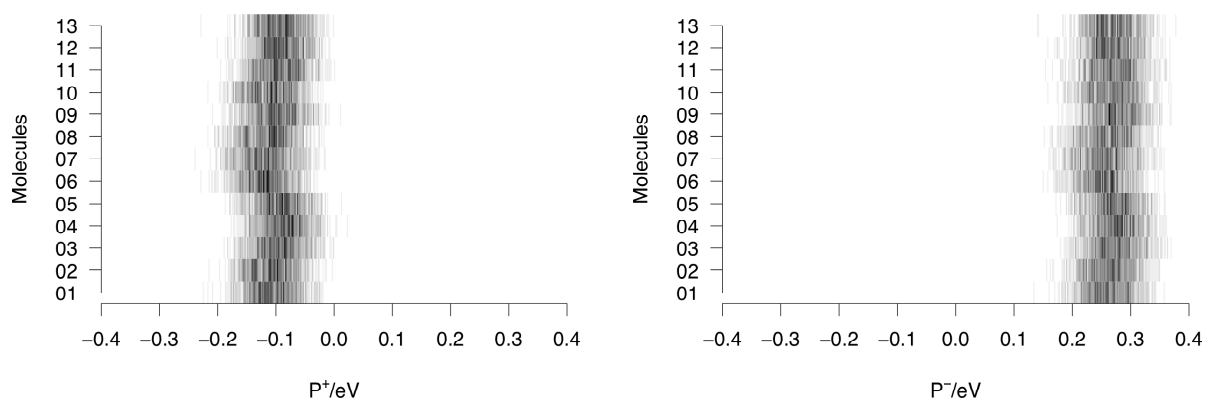


Figure S7: Distributions of the polarization energy for holes (P_i^+ , left) and electrons (P_i^- , right), for each dimer of the unit cell, as calculated at the VB/HF-AM1 level using molecular structures extracted from MD simulations.

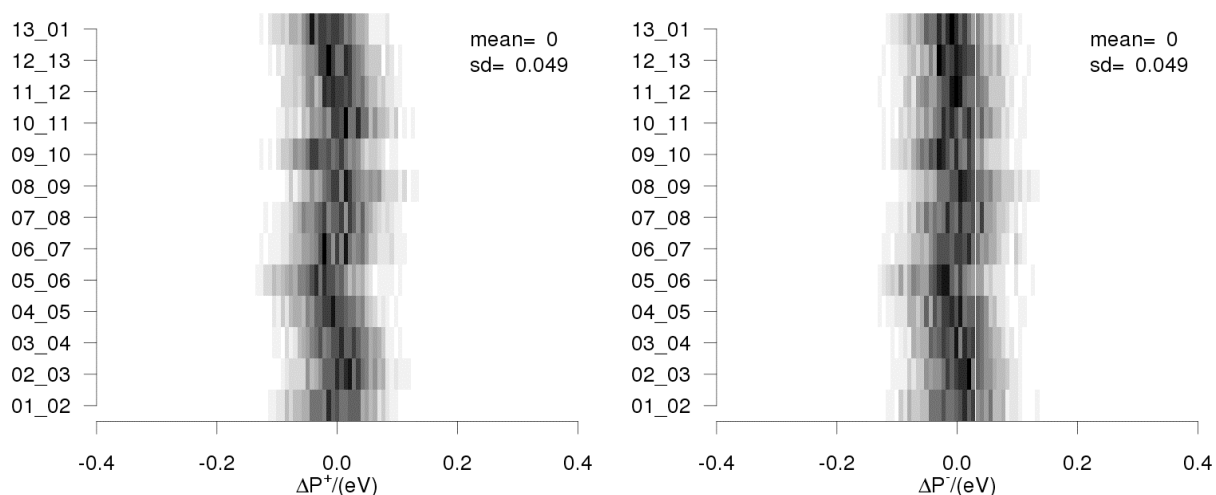


Figure S8: Distributions of the intermolecular energy disorder associated to holes ($\Delta P_i^{+↔}$, left) and electrons ($\Delta P_i^{-↔}$, right) migration, for each dimer of the unit cell, as calculated at the VB/HF-AM1 level using molecular structures extracted from MD simulations.

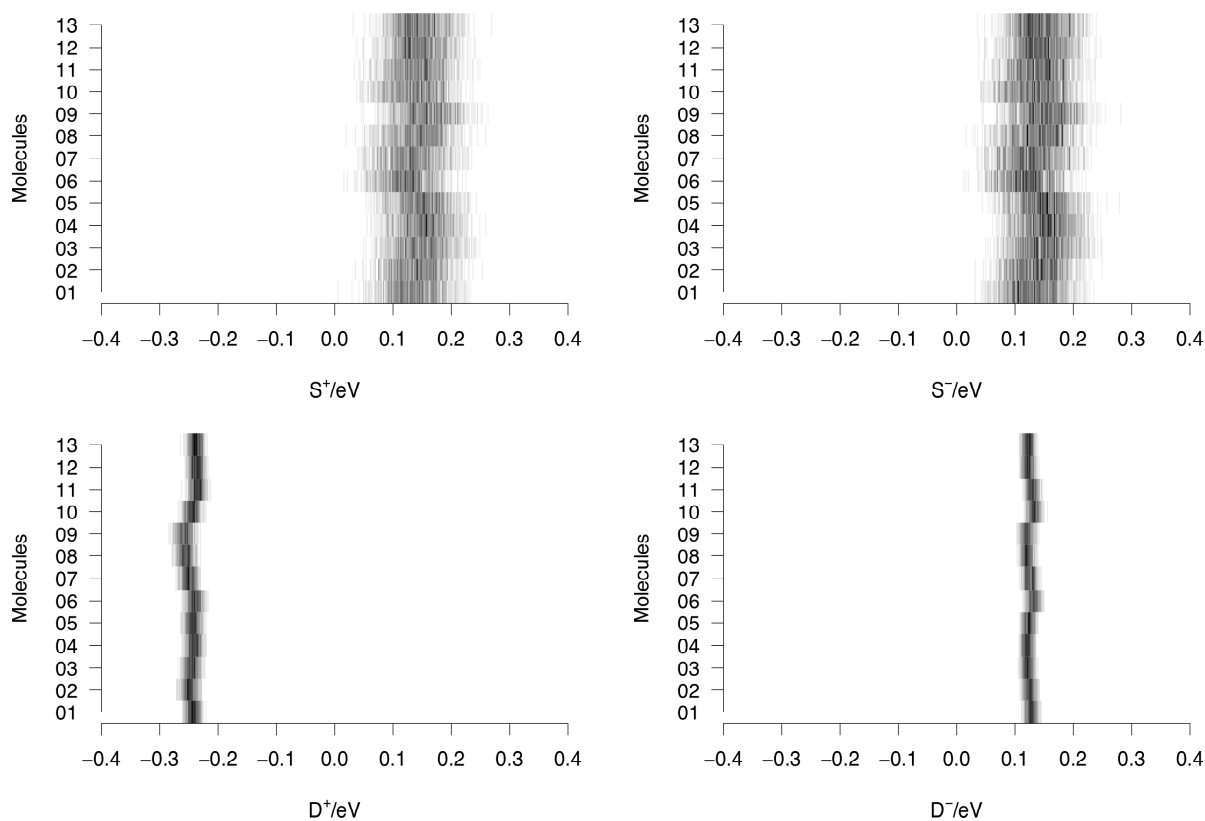


Figure S9: Distributions of the $S^{+/-}$ (top) and $D^{+/-}$ (bottom) contributions to the polarization energy for holes (left) and electrons (right), for each molecule of the unit cell, as calculated at the VB/HF-AM1 level using molecular structures extracted from MD simulations.

2.3. Calculation of the transfer integrals

Comparison of the transfer integrals calculated at the VB/HF and INDO levels

Figure S10 portrays the population of transfer integrals J^+ and J^- between adjacent PDI units in the unit cell, as probed at the VBHF and INDO levels along the MD trajectory. The INDO transfer integrals are ~ 3.5 times larger than the VB/HF ones, while the two levels of calculation lead to very similar distributions.

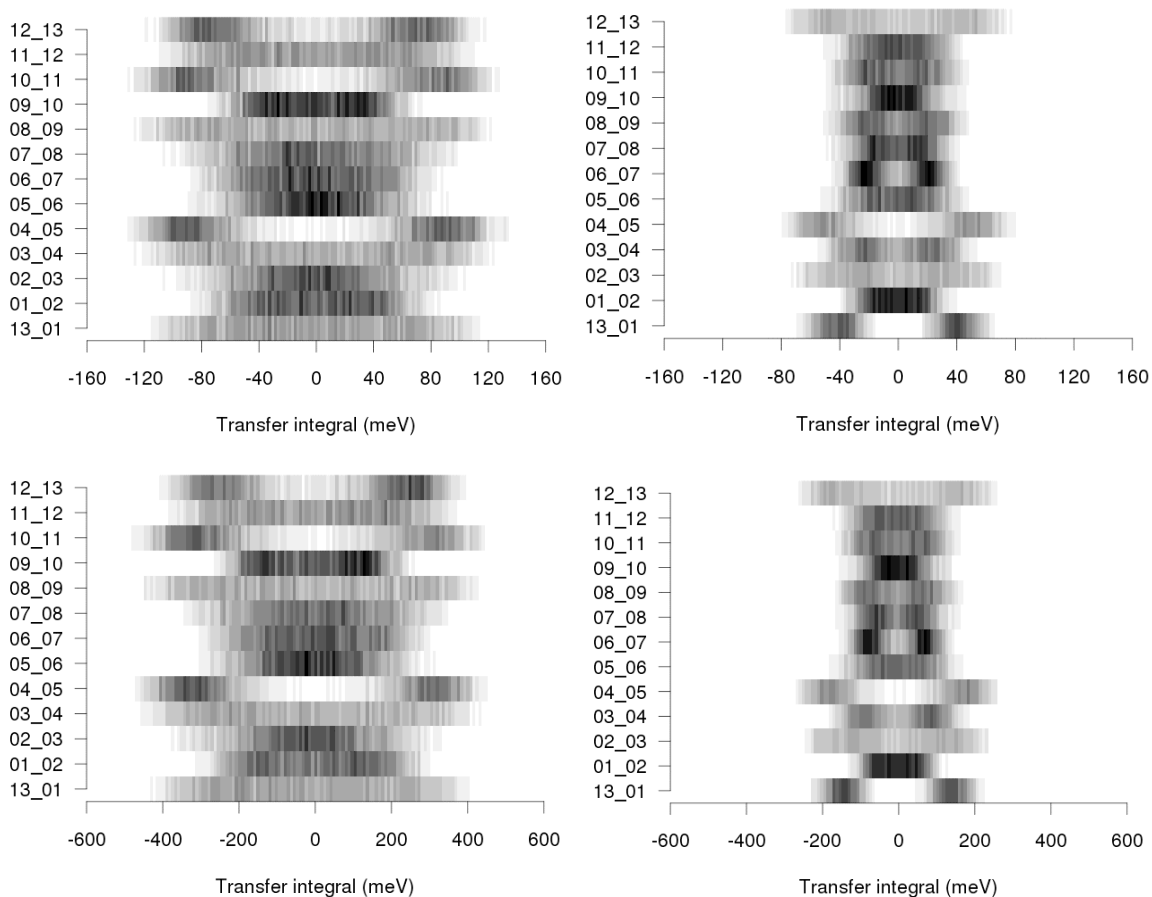


Figure S10: Transfer integral distributions for successive dimers in the stack for holes (left) and electrons (right), as calculated at the VBHF (top) and INDO (bottom) levels.

The variations of J^+ and J^- with respect to the Δx and Δy shifts, as calculated at the VB/HF and INDO levels for the simplified PDI dimer shown in Figure S11, are illustrated in Figure S12. The twist angle θ between the two facing molecules is fixed at 55° . The VB/HF and INDO maps display the same topology, which further confirms that the two levels of approximation lead to similar evolution of the transfer terms with respect to the structural parameters.

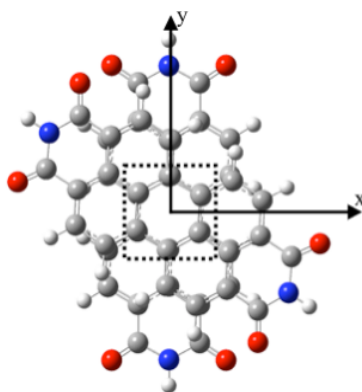


Figure S11: Structure of the model PDI dimer.

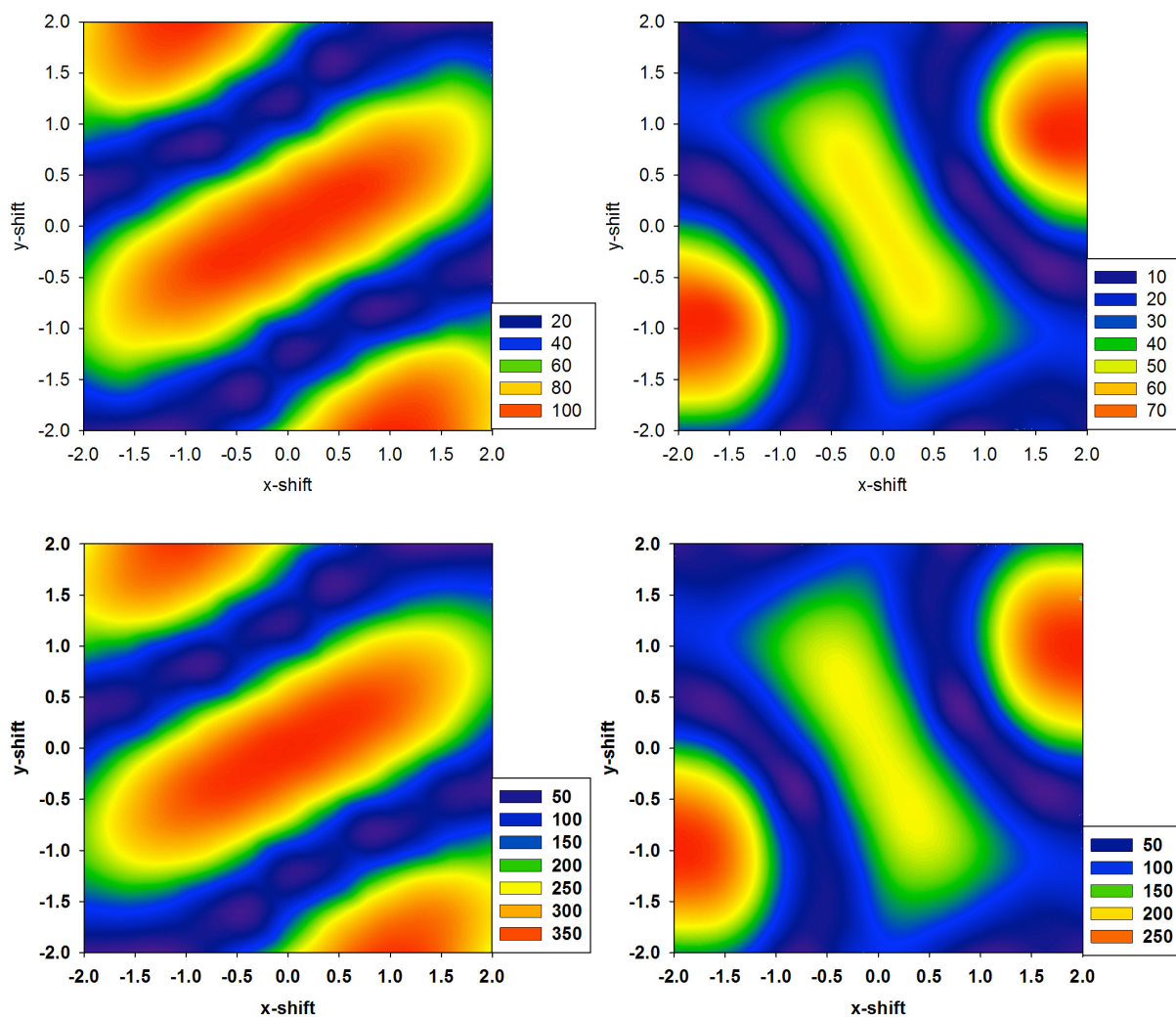


Figure S12: Evolution of J^+ (left) and J (right) in the model dimer with Δx and Δy at the VB/HF (top) and INDO (bottom) levels (in meV).

Evolution of J^+ and J^- with Δx and Δy : charge transfer from molecule 4 to molecule 5.

To complement the investigations on the evolution of J^+ and J^- with the structural parameters provided in Section 4.3 of the article, we consider here, as another representative example, the transfer integrals when the charge hops from molecule 4 to molecule 5 within the unit cell (see Scheme 1). The top of Figure S13 show the values of the relative shifts Δx and Δy sampled along the dynamics superimposed to the color maps of J^+ and J^- calculated at the VB/HF level for the simplified PDI dimer shown in Figure S11. The distributions of the J^+ and J^- values for the dimer 4-5 are portrayed at the bottom of Figure S13.

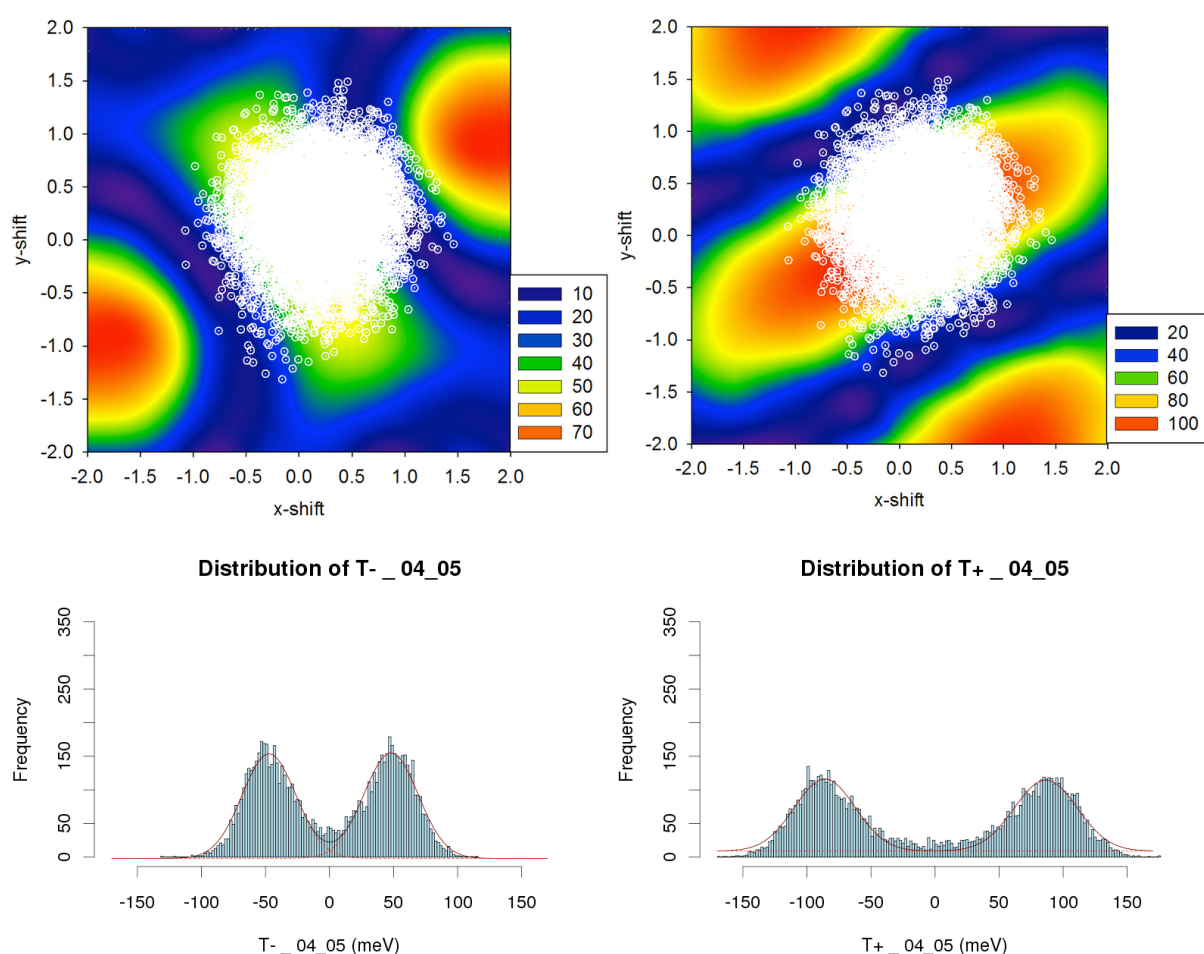


Figure S13: Evolution of J^- (left) and J^+ (right) (in meV) with Δx and Δy (top) in the model dimer, and transfer integral distributions extracted from the MD simulations for a charge migration between molecules 4 and 5 (bottom).

The marked differences between the transfer integral distributions obtained for the dimer 4-5 and for dimer 7-8 (see Figure 7 of the article) can be easily rationalized when considering the differences in the relative positions of the molecules in these two dimers. In

dimer 4-5, the molecule 5 is preferentially located in $\Delta x = 0.23 \text{ \AA}$ and $\Delta y = 0.21 \text{ \AA}$. This geometry favors the overlap between the frontier orbitals of the two monomers, and thus corresponds to a zone associated to high J^+ ($\sim 90 \text{ meV}$), and J^- ($\sim 50 \text{ meV}$) values. In dimer 7-8, the molecule 8 is centered on $\Delta x = -0.17 \text{ \AA}$ and $\Delta y = -1.61 \text{ \AA}$, which associated to small J^+ ($\sim 10 \text{ meV}$) and J^- ($\sim 20 \text{ meV}$) values. In addition, in the region explored by the molecule 5 during the dynamics, the J^+ and J^- maps are more flat than in the region explored by the molecule 8, so that the transfer integrals distributions in dimer 4-5 display a smaller broadening than that obtained for dimer 7-8.

Evolution of J^+ and J^- with Δx , Δy and θ

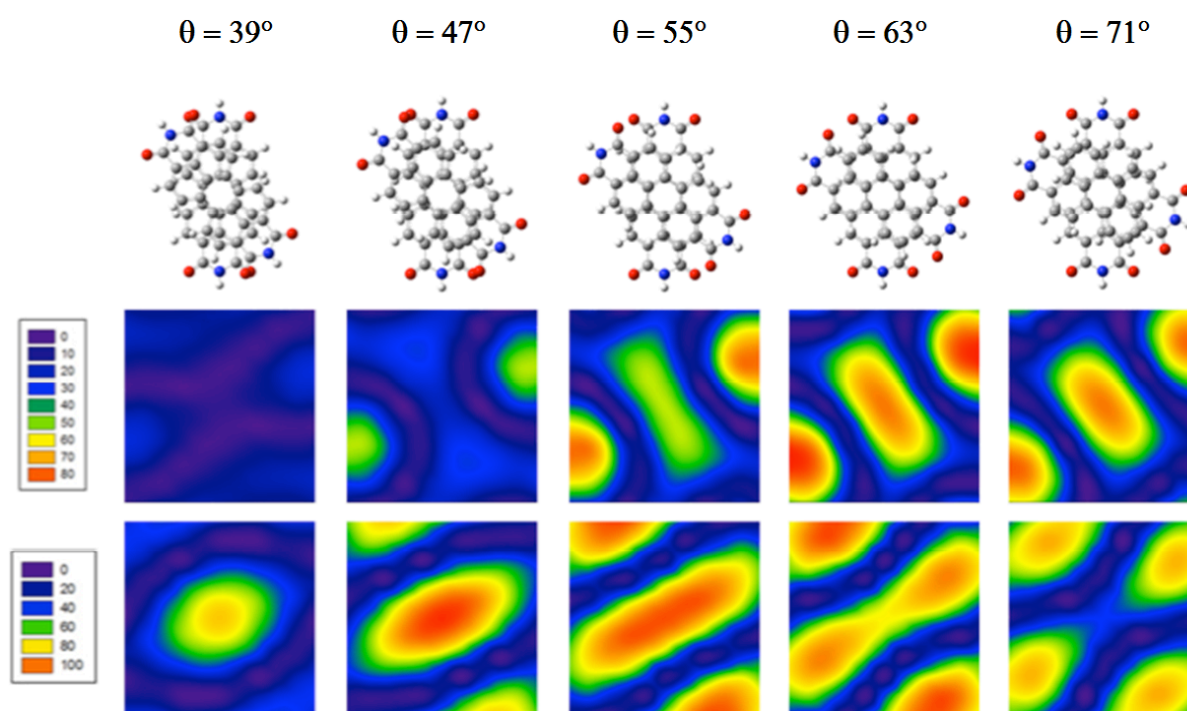


Figure S14: Evolution of the J^- (top) and J^+ (bottom) maps as a function of θ . See also the animated map: [Transfer_integrals_wrt_Theta.gif](#)

Evolution of J^+ and J^- with Δx , Δy and δ

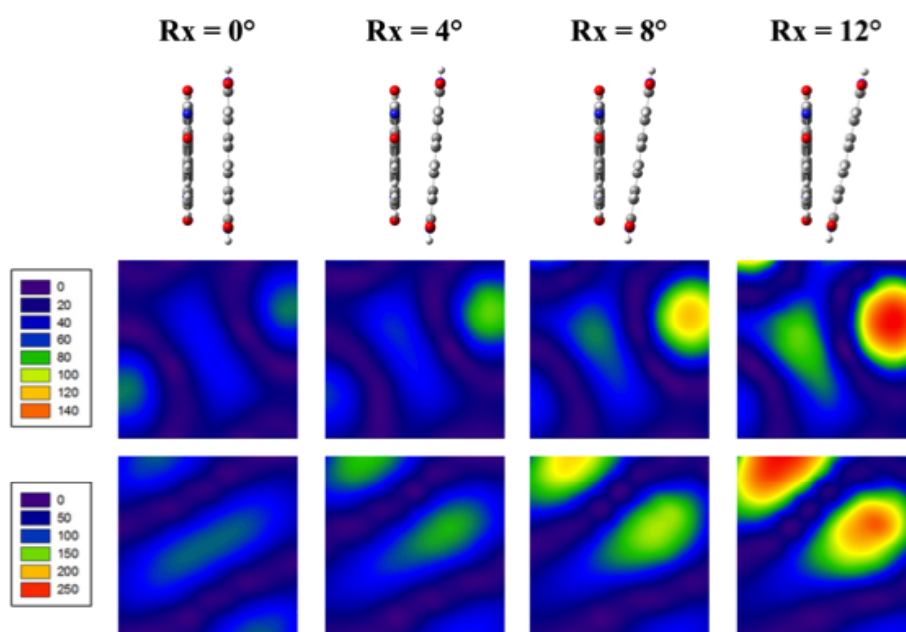


Figure S15: Evolution of the J^- (top) and J^+ (bottom) maps as a function of R_x .
See also the animated map: [Transfer_integrals_wrt_Rx.gif](#)

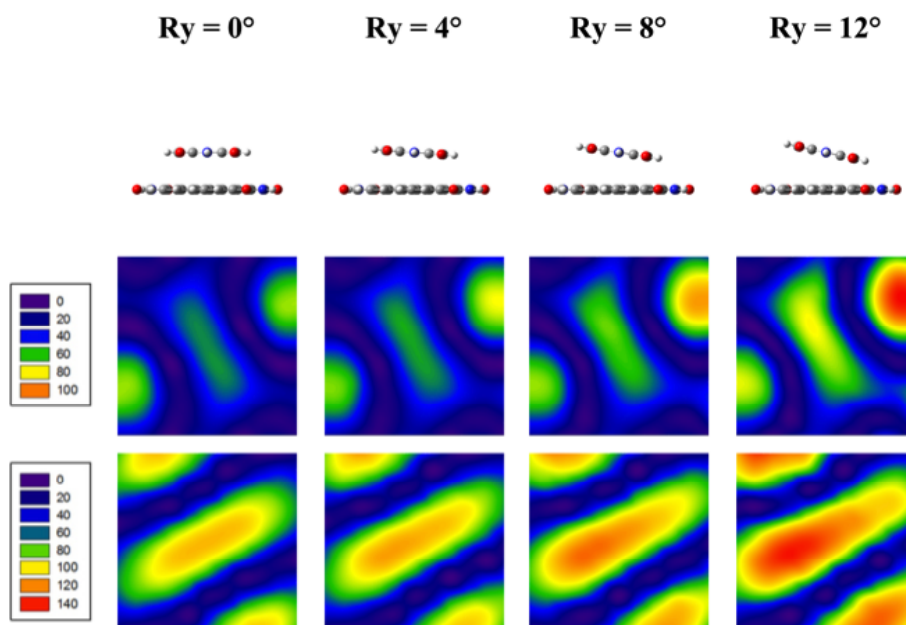


Figure S16: Evolution of J^- (top) and J^+ (bottom) maps as a function of R_y .
See also the animated map: [Transfer_integrals_wrt_Ry.gif](#)

Evolution of J^+ and J^- with Δx , Δy and Δz

See the animated map: [Transfer_integrals_wrt_dz.gif](#)

3. KMC calculations

3.1. Assessment of the convergence of the computed properties

As every stochastic method, the KMC approach requires a large sample of values to converge the simulated properties. In this section, we investigate the number of random shots necessary to get an acceptable convergence of the charge carrier mobilities, with respect to the electric field amplitude used in the simulations. Three different frames extracted from the dynamic, presenting low, high and intermediate mobility values (as determined after a fast calculation using an electric field value of 10^5 V/cm), have been considered. For these three frames, the average mobility values at different electric fields and for different numbers of random shots were calculated. We only report here the results obtained for the frame presenting the intermediate mobility value, without considering any energetic disorder. The averaged mobilities have been calculated by:

$$\langle \mu \rangle = \frac{d}{\langle \tau \rangle F} \quad (\text{S1})$$

where the distance d is equal to 500 nm. Calculations have been performed using $\lambda_s=0.15$ eV and $\lambda_i=0.20$ eV.

The numerical values of the average hole mobilities and the associated standard deviations are reported in Tables S3 and S4, respectively, as a function of the number of random shots, as well as of the amplitude of the applied electric field F . These results show that for an electric field value of 10000 V.cm^{-1} , 50 random shots are sufficient to get a reasonable convergence on the average mobility.

		Electric field/(V.cm ⁻¹)				
		1000	10000	100000	1000000	10000000
# of shots	5	0.0380	0.0294	0.0316	0.0311	0.0121
	10	0.0471	0.0290	0.0323	0.0310	0.0124
	50	0.0399	0.0314	0.0319	0.0310	0.0124
	100	0.0404	0.0318	0.0319	0.0312	0.0123
	1000	0.0413	0.0323	0.0317	0.0313	0.0124
	10000	0.0419	0.0318	0.0317	0.0313	0.0124

Table S3: Average charge carrier mobilities ($\text{cm}^2.\text{V}^{-1}.\text{s}^{-1}$) for different electric fields and values of random shots.

		Electric field/(V.cm ⁻¹)				
		1000	10000	100000	1000000	10000000
# of shots	5	0.0174	0.0082	0.0020	0.0026	0.0007
	10	0.0236	0.0080	0.0030	0.0020	0.0008
	50	0.0316	0.0082	0.0033	0.0018	0.0008
	100	0.0341	0.0093	0.0031	0.0019	0.0007
	1000	0.0326	0.0103	0.0033	0.0018	0.0007
	10000	0.0327	0.0101	0.0033	0.0018	0.0007

Table S4: Standard deviations (cm².V⁻¹.s⁻¹) of the mobility for different electric fields and values of random shots.

3.2. Hole and electron mobilities

λ_s	VB/HF				INDO
	0.05	0.10	0.20	0.30	0.20
<i>static limit</i>					
μ_{h+}	7.80e-04	6.63e-04	3.23e-04	9.18e-05	1.15e-03
μ_{e-}	2.14e-04	9.69e-05	5.58e-05	1.26e-05	2.53e-04
<i>time-averaged limit</i>					
μ_{h+}	1.60e+00	7.43e-01	1.90e-01	5.72e-02	2.25e+00
μ_{e-}	2.02e-01	9.26e-02	2.49e-02	7.96e-03	3.44e-01
<i>space-averaged limit</i>					
μ_{h+}	1.93e+00	8.43e-01	2.27e-01	7.06e-02	2.91e+00
μ_{e-}	2.69e-01	1.17e-01	3.17e-02	9.90e-03	3.79e-01
<i>time-and-space-averaged limit</i>					
μ_{h+}	2.08e+00	8.73e-01	2.37e-01	7.31e-02	3.11e+00
μ_{e-}	2.92e-01	1.27e-01	3.58e-02	1.05e-02	4.48e-01

Table S5: Charge carrier mobilities (in cm².V⁻¹.s⁻¹) in the various limiting cases, as calculated with the KMC scheme using VB/HF and INDO transfer integrals and the average transient time $\langle \tau \rangle$.

4. Autocorrelation functions of the main geometrical parameters

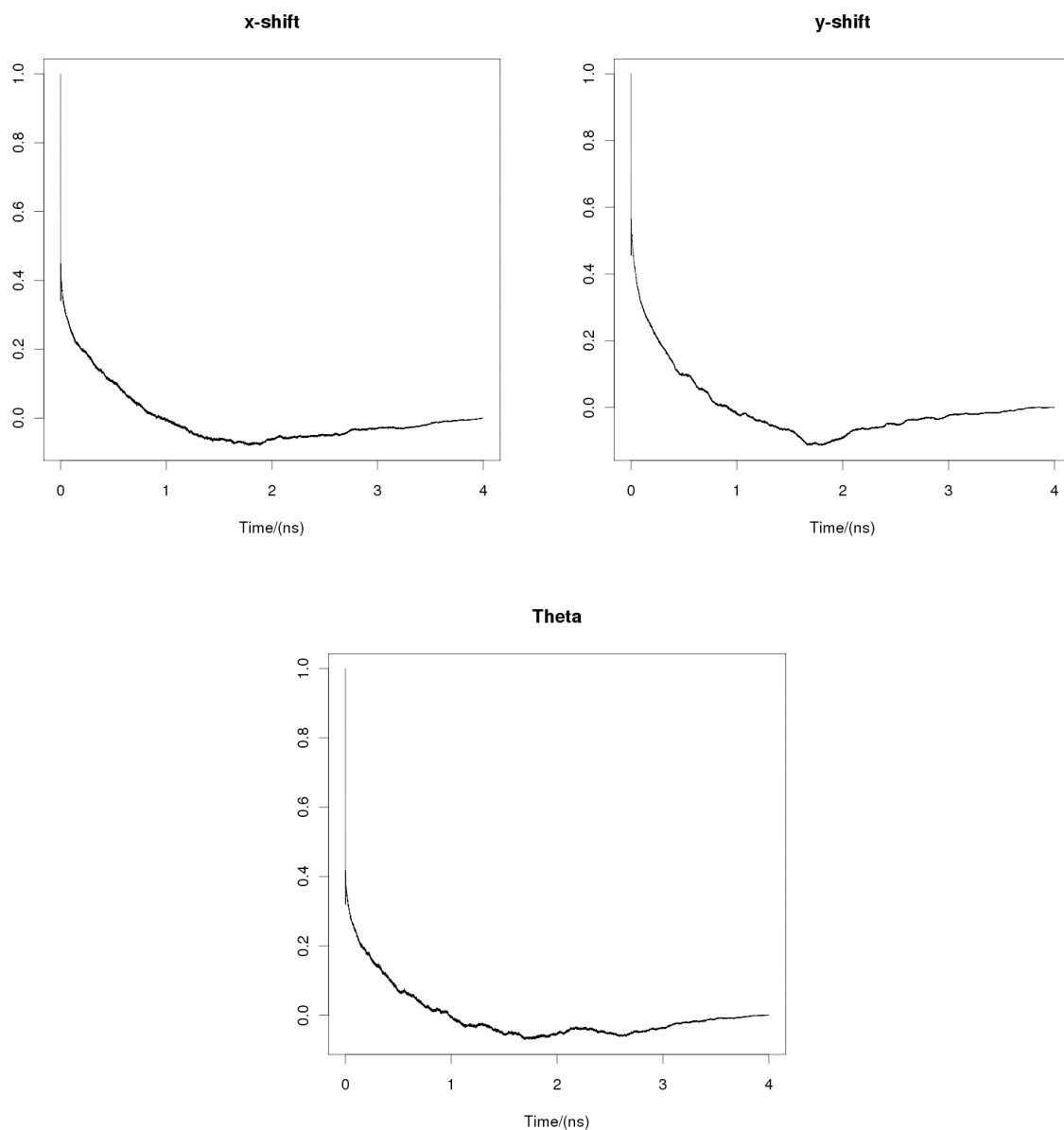


Figure S17: Autocorrelation functions of Δx , Δy and θ .

References

- [Klebe_1988] G. Klebe, F. Graser, E. Hädicke, J. Berndt, *Acta Cryst.* (1989) B45, 69-77.
[Chen_2007] Z. Chen, V. Stepanenko, V. Dehm, P. Prins, L. D. A. Siebbeles, J. Seibt, P. Marquetand, V. Engel, and F. Würthner, *Chem. Eur. J.*, 2007, 13, 436.